TISSUE ENGINEERING: Part A
Volume 15, Number 4, 2009

DOI: 10.1089/ten.tea.2008.0018

Original Articles

Angiogenic Response to Bioactive Glass Promotes Bone Healing in an Irradiated Calvarial Defect

Ann Leu, M.S.,[1] Susanne M. Stieger, D.V.M.,[1,2] Paul Dayton, Ph.D.,[1,*]
Katherine W. Ferrara, Ph.D.,[1] and J. Kent Leach, Ph.D.[1]

Localized radiation is an effective treatment modality for carcinomas, yet the associated reduction of the host vasculature significantly inhibits the tissue's regenerative capacity. Low concentrations of bioactive glass (BG) possess angiogenic potential, and we hypothesized that localized BG presentation would increase neovascularization and promote healing in an irradiated bone defect. An isolated calvarial region of Sprague-Dawley rats was irradiated 2 weeks before surgery. Bilateral critical-sized defects were created and immediately filled with a BG-loaded collagen sponge or an empty sponge as an internal control. Histological analysis of calvaria collected after 2 weeks demonstrated greater neovascularization within the defect in the presence of BG than with collagen alone. Noninvasive ultrasound imaging at 4 weeks detected less contrast agent in the brain below BG-treated defects than in the nearby untreated defects and images of treated defects acquired at 2 weeks. The reduced ability to detect contrast agent in BG-treated defects suggested greater attenuation of ultrasound signal due to early bone formation. Micro-computed tomography imaging at 12 weeks demonstrated significantly greater bone volume fraction within BG-treated defects than in controls. These results suggest that neovascularization induced by localized BG delivery promotes bone regeneration in this highly compromised model of bone healing and may offer an alternative approach to costly growth factors and their potential side-effects.

Introduction

Radiation therapy remains a common postoperative treatment for head and neck cancers. Of the estimated 10.5 million Americans afflicted with or receiving treatment for cancer, approximately half have been treated with radiation therapy, alone or in combination with other therapies.[1] As a result of surgical resection and radiation therapy, these patients commonly suffer loss of additional bone tissue, oftentimes resulting in a slow-healing or nonhealing bone defect that may limit mastication or speech. The combination of radiotherapy and tumor resection, although effective, can therefore lead to potentially harsh physical and associated emotional consequences.

Radiotherapy is an effective strategy to treat malignancies because of its ability to target rapidly dividing cells.[2] However, radiation also inhibits proliferation, migration, and tubule formation of endothelial cells; a deficiency in any of these processes leads to inhibition of neovascularization.[3,4] Although this antiangiogenic effect may be beneficial in antitumor therapy by inhibiting tumor growth,[4] it is counterproductive for the growth and maintenance of healthy tissue, such as bone.[5] In addition to attenuated vascularization, radiation negatively affects a number of other cell types that play a critical role in bone formation and remodeling, including mesenchymal stem cells, osteoblasts, and osteocytes.[6,7] The decrease in osteoblast and osteocyte number disturbs the homeostasis of bone tissue, resulting in a decline in collagen synthesis, matrix formation, and tissue mineralization. The transplantation of vascularized autografts to fill such bone defects remains the criterion standard yet is limited by tissue availability, risk of complications due to additional surgery, and donor site morbidity and pain.[8] Despite their effectiveness in promoting bone healing in otherwise healthy patients, limitations associated with autografts and other graft materials have prompted the search for alternative treatment strategies for bone defects exposed to therapeutic radiation.

Bone tissue development is a highly coordinated process involving the participation of various cell populations and directed by numerous signaling pathways. The systemic or

[1]Department of Biomedical Engineering and [2]School of Veterinary Medicine, University of California at Davis, Davis, California.
*Present address: Joint Department of Biomedical Engineering, University of North Carolina-North Carolina State University, Chapel Hill, North Carolina.

localized delivery of inductive molecules is one of the most widely examined approaches to induce bone healing.[9,10] The local presentation of high concentrations of bone morphogenetic proteins (BMPs) delivered as recombinant proteins[11] or genes encoding for these proteins[12] have exhibited the potential to promote bone formation in irradiated bone defects. However, this approach did not fully overcome the negative effects of irradiation, possibly due to the lack of angiogenic signals. The importance of angiogenesis in bone formation is well described,[13] and the localized delivery of potent angiogenic growth factors such as vascular endothelial growth factor (VEGF) has demonstrated enhanced vascularization and better quality of regenerated bone in healthy models.[14–17] Kaigler *et al.* recently confirmed the benefit of localized VEGF delivery from a polymeric scaffold for inducing angiogenesis and promoting bone formation in irradiated calvarial defects.[18] Still, VEGF plays a large role in tumor angiogenesis, and high concentrations may awaken dormant tumors,[19] thereby limiting the widespread application of this treatment strategy for patients with a history of cancer.

Although bioactive glass (BG) has traditionally been employed for its osteoconductive and osteostimulative properties, recent studies have reported that low concentrations of BG exhibit proangiogenic potential *in vitro*[20,21] and in healthy models *in vivo*.[17,22] Previous studies have reported that the soluble dissolution products of BG up-regulate the production of numerous angiogenic factors by stimulated cells,[20,21] providing a potentially promising strategy to enhance neovascularization and resultant bone formation. Based on its proangiogenic potential, we hypothesized that the localized delivery of BG from a collagen sponge would enhance neovascularization and promote bone formation in an irradiated critical-sized bone defect.

New imaging methods have the potential to greatly enhance preclinical and clinical tissue engineering studies, facilitating noninvasive assessment of tissue properties in deep tissues.[23,24] Historically, laser Doppler flowmeters have been used to assess perfusion; however, these systems are commonly limited to a sampling depth of approximately 1 mm.[25] Estimates of blood volume and microvascular flow rate in deeper tissues can be achieved using ultrasound in combination with highly echogenic intravascular gas bubbles. Tissue echoes, resulting from the transmission of a train of ultrasound pulses with alternating phase, will cancel when summed, but the echoes from the gas bubbles sum partially coherently.[26,27] Here, for the first time, contrast pulse sequencing (CPS® from Siemens) is directed through the bone graft to visualize blood volume over several centimeters in the brain, enabling observation of the attenuation resulting from the developing bone graft. Contrast ultrasound imaging is used clinically to assess wall motion abnormalities, and therefore such methods are not limited in application to small animals or superficial regions.[28] We complement the imaging of blood flow with high-resolution X-ray computed tomography (CT) of the bony defect. With this technique, often called microCT, bone thickness can be assessed *in vitro* or *in vivo* and changes monitored over time.[29]

Materials and Methods

Materials

Bioglass 45S (BG) was from NovaBone Products (Jacksonville, FL) and had a composition of 45.0% silicon dioxide, 24.4% sodium oxide, 24.6% calcium oxide and 6.0% phosphorus pentoxide by weight. Collagen sponges were from Integra LifeSciences (Plainsboro, NJ), and collagen solutions derived from bovine hide were from Inamed Biomaterials (Fremont, CA). All chemicals were from Sigma Aldrich (St. Louis, MO) unless otherwise noted. Immunostaining for von Willebrand Factor (vWF) was achieved following the manufacturer's protocol using a rabbit antihuman vWF primary antibody (1:200 dilution), verified by the supplier to cross-react with rat vascular endothelial cells, and biotinylated antirabbit immunoglobulin (Ig)G contained in a commercial kit by Chemicon (Temecula, CA). Definity ultrasound contrast agent was from Bristol-Myers Squibb Medical Imaging (North Billerica, MA).

Animal irradiation

Treatment of experimental animals was in accordance with the University of California at Davis animal care guidelines and all National Institutes of Health animal handling procedures. Skeletally mature 10-week-old male Sprague-Dawley rats (Taconic Farms, Hudson, NY) were anesthetized with an intraperitoneal injection of a ketamine (80 mg/kg) and xylazine (10 mg/kg) mixture. A single 12-Gy dose from a Varian 2100C linear accelerator (Varian Medical Systems, Palo Alto, CA) was delivered to Dmax at a source-to-skin distance of 80 cm. Prior studies have demonstrated that this is a safe dose for calvarial irradiation in rats.[12,18,30] The pharynx and the rest of the body were shielded using a combination of beam collimation and Cerrobend blocks. Animals were monitored for weight loss, abnormal activity, and hair loss. Similar to previous studies, the radiation dose was given 2 weeks before the surgical procedure.[18,30]

Calvarial defect model

Collagen sponges were loaded with 1.2 mg of BG as previously described.[21] Rats were anesthetized using an intraperitoneal injection of a ketamine–xylazine mixture as described above. A midlongitudinal incision was made on the dorsal surface of the cranium, and care was taken to ensure that the periosteum was completely cleared from the surface of the cranium by scraping. A trephine burr (Ace Dental Implant System, Brockton, MA) was used to create two circular 3.5-mm diameter defects in the rat cranium, one on each side of the sagittal suture. The full thickness of the cranial bone was removed, and BG implants were immediately placed in the right defects; control implants (sponges lacking BG) were placed in the left defects. Some implants were left unfilled to confirm that the defect was critical sized. The incision was closed with a continuous suture (5–0 nylon; Ethicon, Somerville, NJ), and the animals were allowed free access to food and water.

Ultrasound analysis

Ultrasound was used to evaluate neovascularization and bone formation noninvasively at 1, 2, and 4 weeks postsurgery. Rats were anesthetized and maintained using a mixture of isoflurane and oxygen delivered through a mask. The dorsal surface of the head was shaved to yield a proper contact surface, and a 24-gauge catheter was inserted into the tail vein for the injection of the ultrasound contrast agent. Rats

were studied using an Acuson Sequoia 512 ultrasound system (Ultrasound Division, Siemens Medical Solutions, Issaquah, WA) with a 15L8 linear array transducer. The cranial area was covered with acoustic coupling gel, and the transducer was placed dorsally on the head perpendicular to the skull. All rats were initially imaged in B-mode at 14 MHz and a mechanical index of 0.9. The width of the defect at the implantation site was measured using the electronic calipers on the ultrasound system. The transducer was then mechanically fixed with an articulated arm in the parasagittal (1 week postsurgery) or transverse (2 and 4 weeks postsurgery) direction of the head for the remainder of the study. The ultrasound system was set in the CPS imaging mode, and a baseline precontrast image was recorded. CPS balance control was set so that echoes from tissue were mapped to blue pixels, and echoes from contrast agent were mapped to orange. Contrast imaging was subsequently performed using CPS at 8 MHz and a mechanical index of 0.28. The acoustic focus was placed at the level of the defect. The gain settings, pulse repetition frequency, and image compression were left constant in all studies. Contrast ultrasound imaging was performed using a bolus injection of 200 μL of contrast agent followed by 250 μL of sterile saline to flush the entire residual contrast agent out of the catheter. CPS imaging was performed for 3 min, and data were stored on a compact disc and transferred to a personal computer where off-line analysis was performed using MATLAB (Mathworks, Natick, MA). Initial studies confirmed that brain perfusion was not detected through the intact skull (data not shown). Regions of interest were selected around each implant and in brain tissue directly subcranial to each implant. Video intensity corresponding to blood flow was calculated by selecting only orange pixels, which corresponded to signal from the intravascular contrast agent. Mean video intensity per unit area was calculated for each region of interest. The contrast intensity ratio was defined as the contrast agent detected in the brain below control-treated defects:agent detected under defects filled with BG–collagen substrates. Once sufficient bone growth occurs, the propagating ultrasound wave does not traverse the defect at a sufficiently high amplitude to excite the contrast agent, and perfusion is no longer observed along the ultrasound axis distal to the defect. Thus, the contrast intensity ratio decreases as the treated bony defect heals and attenuates the propagating sound.

Histological staining and analysis for neovascularization

Animals were euthanized with carbon dioxide at each time point, and implants were retrieved and fixed for 24 h at 4°C in 10% phosphate buffered formalin. Fixed tissues were bisected through both defects, decalcified in 15% formic acid for 24 h, paraffin-embedded, and sectioned at 6 μm. Two-week sections were stained with hematoxylin and eosin (H&E) or immunostained for vWF, a protein present in large quantities in subendothelial matrices such as blood vessel basement membranes. Sections were imaged using a Nikon Eclipse TE2000U microscope (Melville, NY) and SpotRT digital camera (Diagnostic Instruments, Sterling Heights, MI). Blood vessels in the entire defect, approximately 20 high-power fields, were counted manually at 100× magnification and normalized to tissue area. Blood vessels were identified as circular structures and well-defined long tubule structures, some containing red blood cells. The investigator was blinded to the type of implant present within a defect while counting blood vessels. Tissue sections stained for vWF and counterstained with hematoxylin were used to confirm the location of blood vessels.

In vivo *microCT*

Rats were anesthetized and maintained using a mixture of isoflurane and oxygen delivered through a mask, and the cranial region was imaged using a commercially available microCT scanner (MicroCAT II, Siemens, Knoxville, TN) in standard resolution mode with a 0.5-mm aluminum filter at 4, 8, and 12 weeks postsurgery. Three hundred sixty projections were acquired during a full rotation around the animal with the following scan parameters: 70 KvP, 500 μA, 200 ms per frame, and 30 calibration images (bright and dark fields). The image was reconstructed using the Feldkamp reconstruction algorithm as a 512×512×768 array with corresponding voxel size of 0.097 mm×0.097 mm×0.097 mm. Image resolution was 68 μm.

Ex vivo *microCT*

Week 12 calvarial explants were rescanned using a VivaCT 40 MicroCT scanner (Scanco Medical AG, Brüttisellen, Switzerland) at an energy level of 70 keV, an intensity of 85 μA, and an isotropic resolution of 10.5 μm in all three spatial dimensions. Scanning for the calvarium was initiated proximately 1 mm distal to the defects and extended to cover the entire defects. The right and left defects were evaluated separately. The gray-scale images were segmented using a constrained three-dimensional Gaussian filter ($\sigma = 0.6$, support = 1.0, fixed threshold of 120) to extract the structure of mineralized tissue. Bone volume (BV) was calculated using tetrahedrons corresponding to the enclosed volume of the triangulated surface. Total volume (TV) was the volume of the sample that was examined. A normalized index (BV/TV; bone volume fraction) was used to compare samples of varying size.

After microCT, explanted tissues were decalcified, bisected, and embedded in paraffin. Histological sections (6 μm) were prepared and stained with H&E for general morphology. Histochemical demonstration of alkaline phosphatase activity was performed following a modified version of a previously described method.[31] Briefly, tissue sections were deparaffinized in xylene, hydrated through a graded alcohol series, and preincubated overnight in 1% magnesium chloride in 100 mM Tris-maleate buffer (pH 9.2). Sections were then incubated for 2 h at room temperature in freshly prepared substrate solution (100 mM Tris-maleate buffer, pH 9.2, containing 1.0 mg/mL Fast Red TR and 0.4 mg/mL naphthol AS-MX phosphate [Amresco, Solon, OH]). Control sections were incubated in buffer only. After washing in D1 H_2O, sections were counterstained for 6 min with 0.5% methyl green and mounted with Aquamount (Lerner Laboratories, New York, NY).

Statistical analysis

All data are reported and plotted as means ± standard errors. Statistically significant differences were determined using a paired two-tailed Student *t*-test, and statistical significance was achieved with $p < 0.05$.

Results

BG increases vascularization within irradiated bone defects

An isolated area of calvarium received a therapeutic equivalent 12-Gy dose of radiation from a linear accelerator. All animals were monitored closely before and up to 12 weeks after surgery. Aside from partial hair loss, there were no observed side effects with any animals. Two weeks after irradiation, two 3.5-mm osseous defects were created in the irradiated site and immediately filled with a BG-loaded and control collagen sponge (Fig. 1). The flexible mechanical properties of the collagen sponge enabled placement of the constructs immediately adjacent to all aspects of the bone defect. Two weeks after implantation, tissues were retrieved, processed, and stained with H&E, and blood vessels were manually counted (Fig. 2A, B). Blood vessels were identified as circular structures and well-defined long tubule structures, some containing red blood cells. vWF staining was used to confirm the presence of blood vessels (data not shown). Analysis of tissue sections 2 weeks after implantation revealed greater vascular density within defects treated with BG (35 ± 16 vessels/mm^2) than in controls (12 ± 2 vessels/mm^2; $n = 6$; $p = 0.09$) (Fig. 2C). Nearly all animals exhibited substantially greater vascularization in the presence of BG, although one animal had a higher vessel density in the control region (13.1 vessels/mm^2) than in the BG-treated region (3.1 vessels/mm^2).

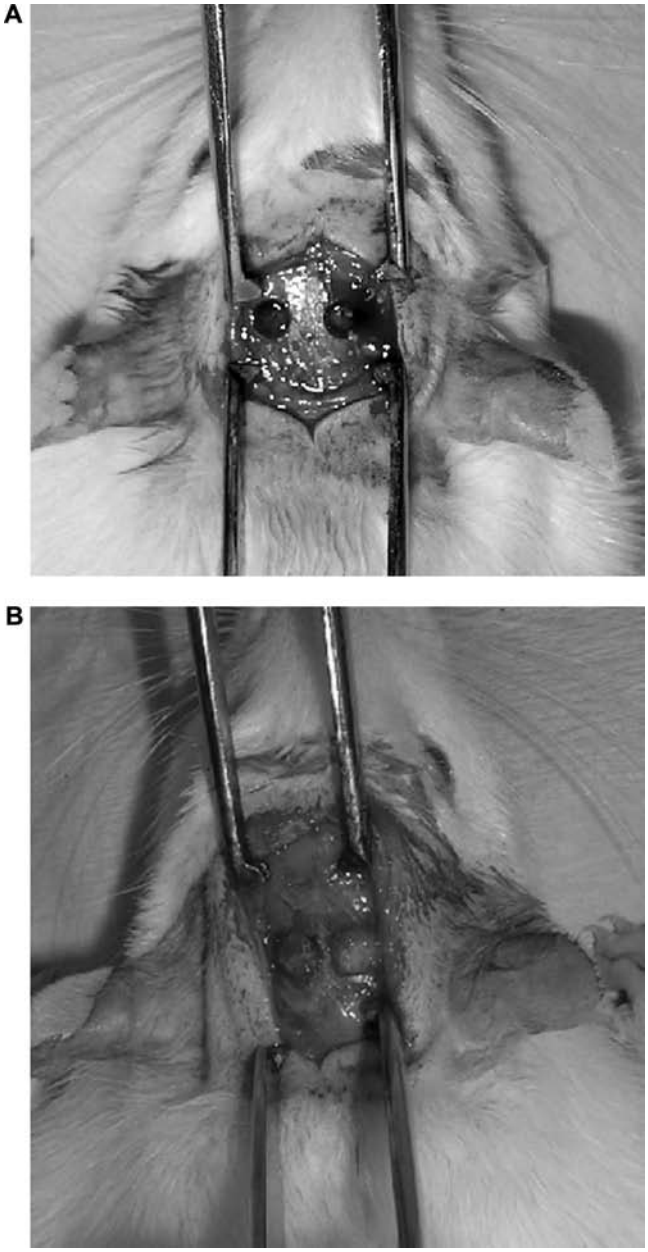

FIG. 1. (**A**) Bilateral defects (3.5 mm in diameter) created in the calvarial region of a rat. (**B**) Bilateral defects containing a collagen sponge (left) and a bioactive glass–collagen sponge (right).

At 1, 2, and 4 weeks, rats were noninvasively examined using ultrasound imaging techniques in CPS mode. Because of the resolution of the images, it was difficult to detect and quantify perfusion within the defects. However, contrast agent within the brain beneath the defects could be prominently seen, more so on the control side than on the BG-treated side. We assumed the presence of contrast agent to be indicative of perfusion, because the agent was administered systemically through the tail vein. The ratio of contrast intensity below the control and the treated detect was then calculated. Although the defect and implants were easily visualized, no qualitative differences in cranial perfusion could be seen at week 1 (images not shown), indicating that it was too early to detect differences in vascularization or bone formation. At weeks 2 and 4, transverse views containing both defects were imaged before (Fig. 3A) and after (Fig. 3B) delivery of contrast agent. Greater asymmetry was observed in week 4 than in week 2 in perfusion underlying the control and treated defects as a result of the attenuation of the wave traversing the treated defect (right side). Therefore, the contrast intensity ratio for 4 weeks postsurgery increased markedly because of the inability to detect contrast agent below the BG-treated defect. These findings establish that the ultrasound signal was more attenuated on the BG-treated side than the control side at later time points, suggesting early bone formation (Fig. 3C).

Analysis of bone regeneration

In vivo microCT was used to screen for bone formation over time in a constant cohort of animals ($n = 6$) at 4, 8, and 12 weeks postsurgery. We observed substantial increases in bone coverage in BG-treated defects, some as early as 4 weeks, and newly formed mineralized tissue remained over the 12-week duration (Fig. 4A). According to qualitative inspection of reconstructed microCT images, all but one rat exhibited more bone coverage in the BG-treated defect than the control at 12 weeks. Furthermore, defects containing no implant displayed no mineralized tissue formation or defect closure, verifying that the defect was critical sized (data not shown).

Reconstructed microCT images obtained from the scanning of explanted calvarial tissue 12 weeks postsurgery enabled a view of the defects at a higher resolution (Fig. 4B). Data obtained from these scans were used to generate three-dimensional reconstructions of the volume of mineralized tissue within each region. Using software associated with the scanning hardware, bone volume fraction (BVF) was

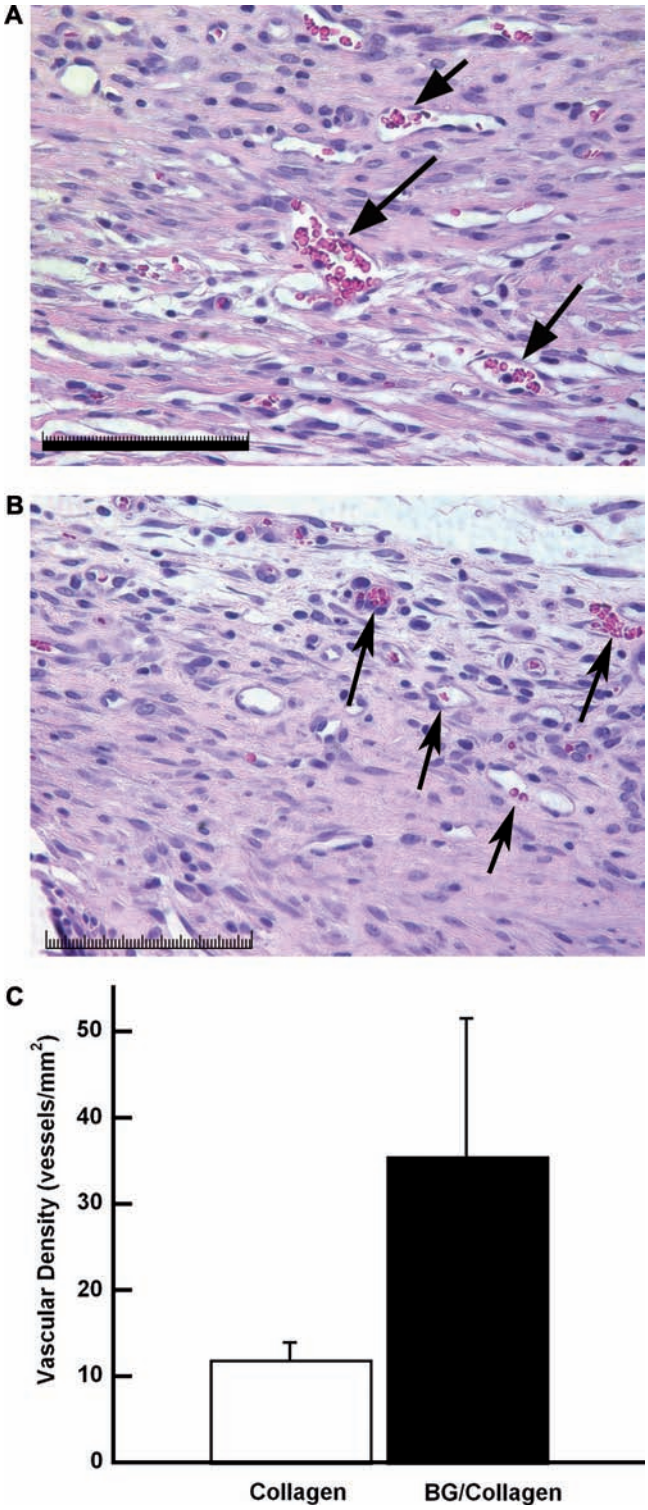

FIG. 2. Two-week decalcified tissues stained with hematoxylin and eosin and treated with the bioactive glass (BG)-loaded collagen sponge (**A**) or collagen control (**B**) and imaged at 40×. Arrows denote vessels; scale bar represents 100 μm. (**C**) Quantification of blood vessel density of the collagen control sponges (open bar), and the BG-loaded collagen sponges (filled bar). Data are means ± standard errors of the mean. Color images available online at www.liebertonline.com/ten.

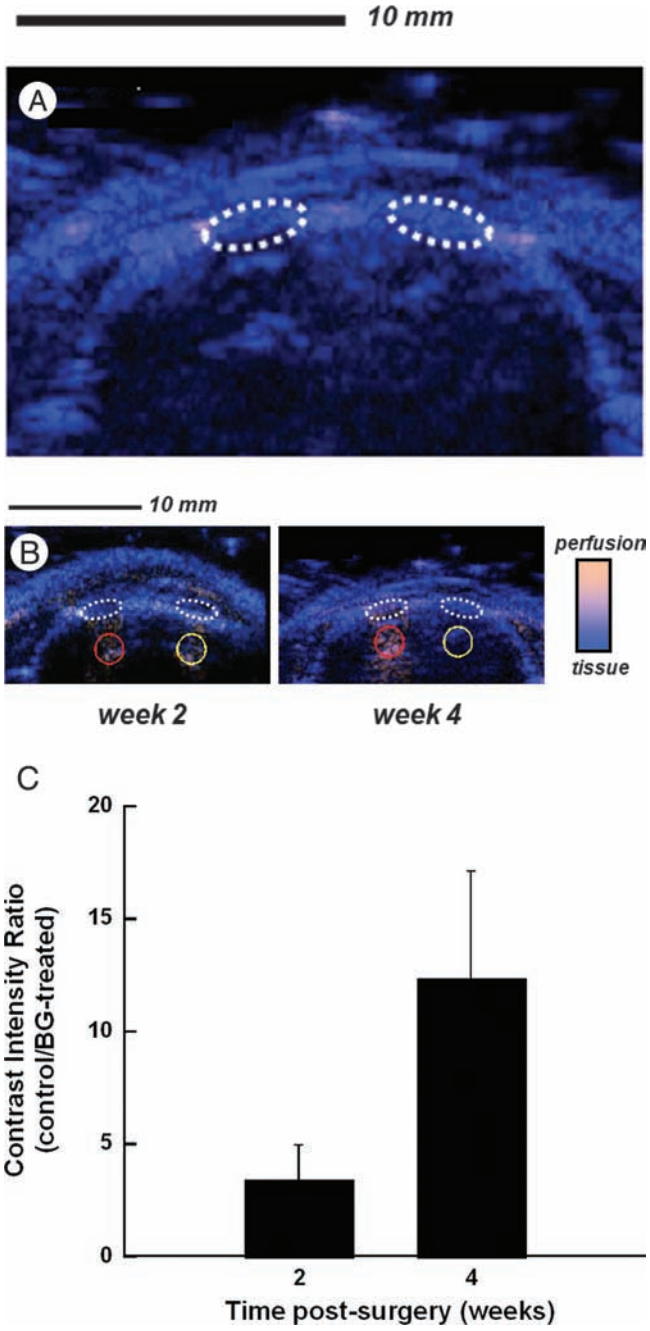

FIG. 3. (**A**) Representative transverse ultrasound image of bilateral calvarial defect under contrast pulse sequencing (CPS) mode at 4 weeks before delivery of contrast agent. Defect areas are denoted by dashed lines. (**B**) Representative transverse ultrasound images of bilateral calvarial defect under CPS mode 5 s after the delivery of contrast agent at 2 and 4 weeks postsurgery. The defect on the right contains a bioactive glass (BG)-loaded collagen sponge; the left defect is filled with an empty collagen sponge. Defect areas are denoted by dashed lines, and perfusion regions of interest are denoted by red and yellow circles for control and BG treatment, respectively. Color scale bar represents differences in echogenicity related to perfusion and surrounding tissues. (**C**) Contrast intensity ratio as a function of time, defined as the ratio of contrast agent detected in the brain below control defects to BG-treated defects. Data are means ± standard errors of the mean. Color images available online at www.liebertonline.com/ten.

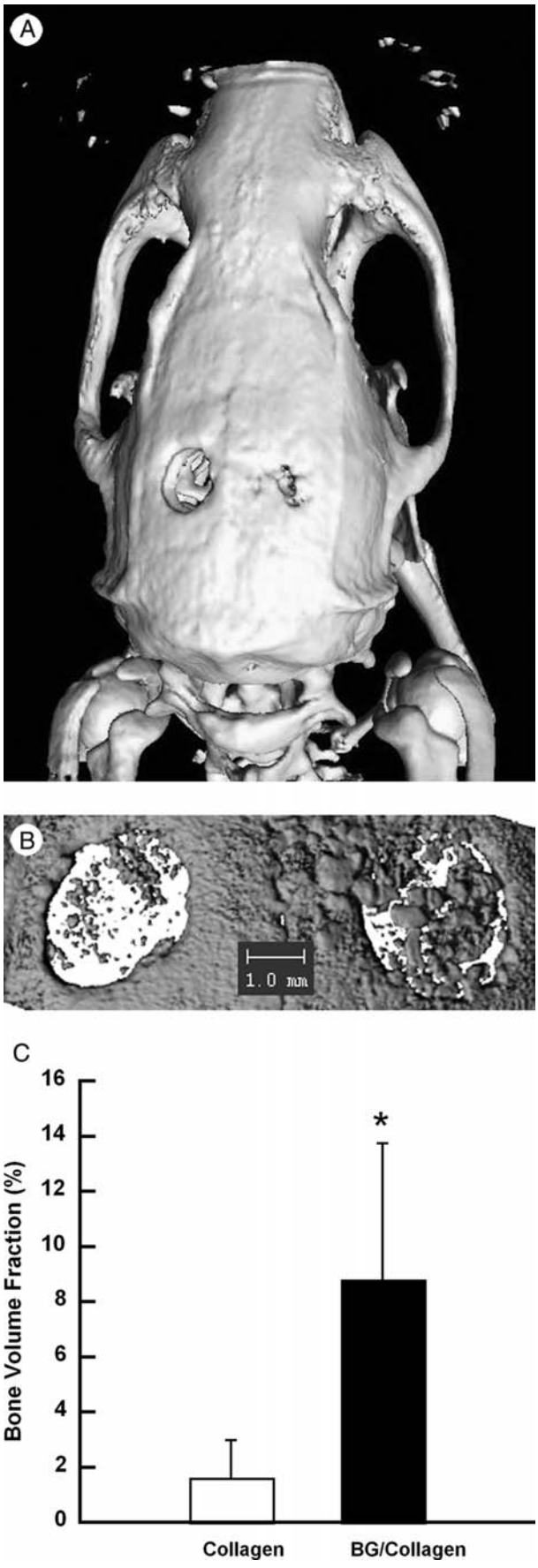

determined for each sample. BG-treated defects exhibited statistically significantly greater BVF ($8.8 \pm 2.0\%$; $p < 0.01$; $n = 6$) than control-treated defects ($1.6 \pm 0.55\%$) (Fig. 4C).

Bone defects treated with a collagen sponge alone showed minimal bone apposition and highly disorganized tissue, whereas BG-treated defects exhibited mineralized nodules distributed throughout the defect area (Fig. 5A). These tissues were subsequently stained for alkaline phosphatase to determine the presence of active osteoblasts. Unlike control-treated defects (Fig. 5B), alkaline phosphatase staining was visibly apparent in BG-treated defects and localized near mineralized nodules (Fig. 5C), suggesting the presence of cells from the bone lineage that was driving new bone formation.

Discussion

The results of these studies confirm the angiogenic potential of low concentrations of BG. Moreover, BG-induced angiogenesis has the potential to enhance bone healing in this severely compromised model of bone healing. Traditional strategies to promote bone regeneration commonly deliver soluble osteogenic signals such as BMPs to induce differentiation of neighboring osteoprogenitor cells.[10] Despite the success of this strategy in otherwise healthy patients, those who have undergone radiation therapy often experience delayed or reduced healing of bone defects, probably resulting from compromised vasculature.

In light of the importance of angiogenesis in bone formation, the presentation of proangiogenic signals has been explored as a potential approach in the field of bone tissue engineering. VEGF seems to be an obvious choice for re-establishing a vasculature because of its potent angiogenic properties. After the implantation of a VEGF-releasing polymeric scaffold, Kaigler *et al.* reported greater vascularization in an identical irradiated calvarial defect model, which resulted in greater bone coverage and bone mineral density.[18] However, patients with a history of cancer may experience adverse effects from this treatment strategy, including tumor recurrence,[19,32] thereby necessitating alternative approaches to effectively induce localized angiogenesis.

The results of these studies demonstrate a novel approach for enhancing vascularization within an irradiated bone defect through localized delivery of bioactive glass. The proangiogenic potential of this hybrid construct was previously demonstrated *in vitro*;[21] the greatest endothelial cell proliferation and tubule formation was observed using collagen sponges loaded with 1.2 mg of BG. In these studies, we observed a trend toward greater neovascularization (nearly 3-fold, on average) within irradiated bone defects treated with BG than in controls at 2 weeks. This finding is in agreement

FIG. 4. (**A**) Representative *in vivo* micro computed tomography (CT) image of calvaria at 12 weeks postsurgery. (**B**) Representative *ex vivo* microCT image of explanted calvaria 12 weeks postsurgery. Left defect filled with collagen sponge; right defect filled with bioactive glass (BG)-loaded collagen sponge. (**C**) Quantitative analysis of bone volume fraction in collagen control implants (open bar) and BG-loaded collagen implants (filled bar). Data are means ± standard errors of the mean. $^*P < 0.01$ versus collagen control implants.

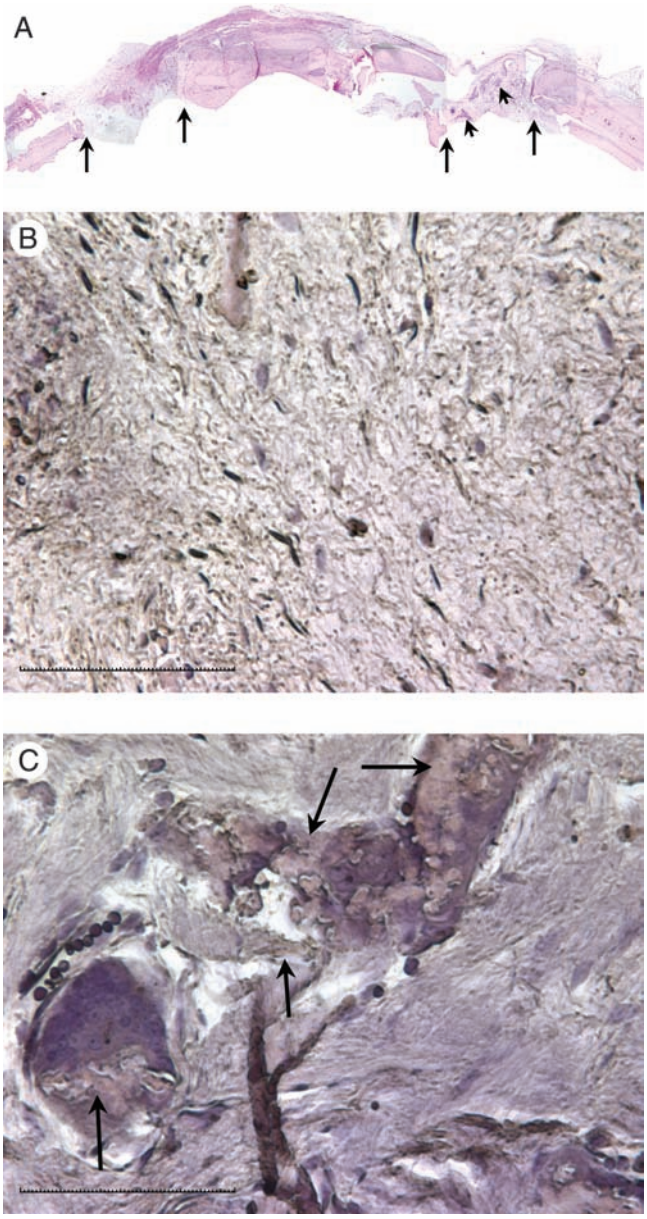

FIG. 5. (**A**) Representative decalcified tissue at 12 weeks postsurgery stained with hematoxylin and eosin. Arrows denote margins of remaining defects treated using an empty collagen sponge (left) or a bioactive glass (BG)-loaded collagen sponge (right); arrowheads denote islands of mineralized nodules within BG-treated defects. Empty collagen sponges lack localized positive staining for alkaline phosphatase (**B**), whereas alkaline phosphatase staining of BG-treated defects confirms the presence of cells from the osteogenic lineage, as represented by reddish-brown staining (arrows) (**C**). 40× magnification; scale bar represents 100 μm. Color images available online at www.liebertonline.com/ten.

with previous studies that demonstrated the potential to enhance neovascularization using VEGF in this identical model.[18] The delivery of VEGF involves the presentation of one signal that, although robust, is not representative of the multitude of signals that naturally occur in wound repair and tissue regeneration. Reports from our laboratory[21] and others[20,33] show that the soluble dissolution products of BG up-regulate the secretion of angiogenic factors (e.g., VEGF and basic fibroblast growth factor) by stimulated cells. Furthermore, several studies have reported greater tissue formation after the localized delivery of multiple, synergistic soluble signals,[34–36] suggesting that cooperative delivery strategies have significant advantages over presenting individual factors.

Similar to previous studies in healthy[14,15,17] or compromised models of bone repair,[18] we observed that greater angiogenesis resulted in enhanced bone formation. BVF measurements collected using *ex vivo* microCT revealed significantly greater new bone formation (more than 5-fold) than in collagen controls. This relative change is substantially greater than those observed when delivering angiogenic growth factors in nonimpaired models of bone repair[15,17] and is comparable with bone formation in response to the sustained delivery of VEGF in an irradiated bone defect.[18] Similar to the natural formation of collateral blood vessels in soft tissues in response to ischemia, these differences suggest that significant effects on neovascularization-related tissue formation may be achievable through less angiogenic stimulation.

Historically, the use of BG as a bone grafting material has commonly required packing of the full defect with BG, resulting in exponentially greater particulate content than in this study. Neighboring progenitor cells and cells of the osteogenic lineage may then colonize this osteoconductive material and initiate the formation of mineralized tissues. Although higher concentrations of BG have demonstrated enhanced osteogenic potential upon exposure to cells of the osteogenic lineage in culture,[37] previous studies *in vitro* suggest that the mass of BG used in this study does not exhibit robust osteogenic potential.[21] Specifically, we did not detect more alkaline phosphatase than in blank sponges using this BG dosage, and we observed greater osteodifferentiation of MC3T3-E1 murine preosteoblasts only when seeded on collagen sponges containing 12 mg of BG. This discrepancy suggests that osteogenesis in this model is occurring through an alternate mechanism. In addition to promoting angiogenesis, trophic factors secreted by BG-stimulated cells may also affect cells of the osteogenic lineage such as mesenchymal stem cells, osteoblasts, and osteocytes. Differentiating osteoblasts expressed VEGF, along with its receptors (VEGFR-1 and VEGFR-2),[38] which has also demonstrated the ability to act as a potent chemoattractant to induce the migration[39] and proliferation[40] of osteoblasts. The direct effect of VEGF on the differentiation of osteoblastic precursors is less clear. Villars *et al.* concluded that VEGF did not directly affect the differentiation of human bone marrow stromal cells.[41] However, Kaigler *et al.* demonstrated a clear increase in osteogenesis when BMSCs were cultured[42] and transplanted[43] in direct contact with endothelial cells, a cellular population known to secrete VEGF under hypoxic conditions present during bone repair.[44]

Noninvasive imaging of perfusion using ultrasound has been effectively used in soft tissue[45–47] but has yet to be successfully applied in a bone defect. In this study, contrast-enhanced ultrasound did not ultimately reveal any definitive information about neovascularization within the bone defect, largely because of the inability to image individual blood vessels at the necessary resolution. However, we detected significant differences in the amount of contrast agent below each defect, with these differences becoming more pronounced over time (Fig. 3). The attenuation of the ultrasound signal on the BG-treated side was most likely due to new bone

formation and not interference by BG, because this phenomenon was not observed at week 1. Ultrasound, although originally intended for noninvasive examination of neovascularization, proves to be an alternative technique to costly microCT scans or potentially problematic X-rays in detecting early bone formation.

The timing of irradiation is an important consideration when examining strategies to promote bone repair in compromised models of bone healing. Successful bone regeneration has been achieved after preoperative radiation with localized angiogenic (e.g., VEGF) or osteoinductive (e.g., BMP-7) therapies,[18,30] and the studies described herein were designed to compare our findings with these reports. Nussenbaum *et al.* reported significantly greater bone regeneration with postoperative radiation than with preoperative radiation when transplanting BMP-7-producing fibroblasts in the identical experimental model.[12] The authors suggested that the delay before radiation allowed sufficient osteoinduction within the 2-week period to initiate the regenerative process. Based on the reported studies herein, we further hypothesize that these differences may be related to the establishment of a capillary network shortly after cell transplantation that is capable of supporting fibroblast survival and robust BMP-7 production for 2 weeks. After radiation, that network is largely destroyed, resulting in cell death and a loss of BMP-7 presentation. The capacity of BG-induced angiogenesis to withstand postoperative radiation is presently unknown and represents an important future study to determine the clinical applicability of this approach.

These studies confirm that a biomaterial-based strategy is sufficient to improve vascularization in a highly compromised model of bone healing. Increases in blood vessel density corresponded with significantly better bone formation. Although the level of secreted angiogenic factors by stimulated cells is low, the potential adverse effects of localized BG-mediated angiogenic factor presentation may be problematic for patients with residual disease, which necessitates further studies in a tumor-challenged model before clinical application. Better results may be achievable if BG is used in conjunction with the delivery of soluble osteogenic molecules such as BMP-2 or BMP-7 or allograft implants. The mass of BG necessary to induce a sufficient angiogenic response represents a substantial cost savings over recombinant growth factors while possessing superior long-term stability. Therefore, a biomaterial-based strategy to induce angiogenesis may provide a novel method for improving bone regeneration within previously irradiated bone defects.

Acknowledgments

The authors thank Michael Kent for assistance with irradiation; Jennifer Fung, Wei Yao, and Nancy Lane for assistance with microCT; Jiawei He for technical assistance; and Damian Genetos for helpful suggestions on this manuscript. The authors acknowledge financial support from the American Cancer Society and the Dean, University of California at Davis School of Medicine [notice ACS IRG-95-125-07].

References

1. American Cancer Society. Cancer Facts & Figures 2008. Atlanta: American Cancer Society, 2008.
2. Stone, H.B., Coleman, C.N., Anscher, M.S., and McBride, W.H. Effects of radiation on normal tissue: consequences and mechanisms. Lancet Oncol **4,** 529, 2003.
3. Udagawa, T., Birsner, A.E., Wood, M., and D'Amato, R.J. Chronic suppression of angiogenesis following radiation exposure is independent of hematopoietic reconstitution. Cancer Res **67,** 2040, 2007.
4. Abdollahi, A., Lipson, K.E., Han, X., Krempien, R., Trinh, T., Weber, K.J., Hahnfeldt, P., Hlatky, L., Debus, J., Howlett, A.R., and Huber, P.E. SU5416 and SU6668 attenuate the angiogenic effects of radiation-induced tumor cell growth factor production and amplify the direct anti-endothelial action of radiation *in vitro*. Cancer Res **63,** 3755, 2003.
5. Okunieff, P., Wang, X., Rubin, P., Finkelstein, J.N., Constine, L.S., and Ding, I. Radiation-induced changes in bone perfusion and angiogenesis. Int J Radiat Oncol Biol Phys **42,** 885, 1998.
6. Li, J., Kwong, D.L.W., and Chan, G.C.F. The effects of various irradiation doses on the growth and differentiation of marrow-derived human mesenchymal stromal cells. Pediatr Transplant **11,** 379, 2007.
7. Dudziak, M.E., Saadeh, P.B., Mehrara, B.J., Steinbrech, D.S., Greenwald, J.A., Gittes, G.K., and Longaker, M.T. The effects of ionizing radiation on osteoblast-like cells *in vitro*. Plast Reconstr Surg **106,** 1049, 2000.
8. Arrington, E.D., Smith, W.J., Chambers, H.G., Bucknell, A.L., and Davino, N.A. Complications of iliac crest bone graft harvesting. Clin Orthop Relat Res, 300, 1996.
9. Lieberman, J.R., Daluiski, A., and Einhorn, T.A. The role of growth factors in the repair of bone. Biology and clinical applications. J Bone Joint Surg Am **84-A,** 1032, 2002.
10. Leach, J.K., and Mooney, D.J. Bone engineering by controlled delivery of osteoinductive molecules and cells. Expert Opin Biol Ther **4,** 1015, 2004.
11. Wurzler, K.K., DeWeese, T.L., Sebald, W., and Reddi, A.H. Radiation-induced impairment of bone healing can be overcome by recombinant human bone morphogenetic protein-2. J Craniofac Surg **9,** 131, 1998.
12. Nussenbaum, B., Rutherford, R.B., Teknos, T.N., Dornfeld, K.J., and Krebsbach, P.H. Ex vivo gene therapy for skeletal regeneration in cranial defects compromised by postoperative radiotherapy. Hum Gene Ther **14,** 1107, 2003.
13. Carano, R.A., and Filvaroff, E.H. Angiogenesis and bone repair. Drug Discov Today **8,** 980, 2003.
14. Street, J., Bao, M., deGuzman, L., Bunting, S., Peale, F.V., Jr., Ferrara, N., Steinmetz, H., Hoeffel, J., Cleland, J.L., Daugherty, A., van Bruggen, N., Redmond, H.P., Carano, R.A., and Filvaroff, E.H. Vascular endothelial growth factor stimulates bone repair by promoting angiogenesis and bone turnover. Proc Natl Acad Sci U S A **99,** 9656, 2002.
15. Murphy, W.L., Simmons, C.A., Kaigler, D., and Mooney, D.J. Bone regeneration via a mineral substrate and induced angiogenesis. J Dent Res **83,** 204, 2004.
16. Kleinheinz, J., Stratmann, U., Joos, U., and Wiesmann, H.P. VEGF-activated angiogenesis during bone regeneration. J Oral Maxillofac Surg **63,** 1310, 2005.
17. Leach, J.K., Kaigler, D., Wang, Z., Krebsbach, P.H., and Mooney, D.J. Coating of VEGF-releasing scaffolds with bioactive glass for angiogenesis and bone regeneration. Biomaterials **27,** 3249, 2006.
18. Kaigler, D., Wang, Z., Horger, K., Mooney, D.J., and Krebsbach, P.H. VEGF scaffolds enhance angiogenesis and bone regeneration in irradiated osseous defects. J Bone Miner Res **21,** 735, 2006.

19. Hicklin, D.J., and Ellis, L.M. Role of the vascular endothelial growth factor pathway in tumor growth and angiogenesis. J Clin Oncol **23,** 1011, 2005.
20. Day, R.M. Bioactive glass stimulates the secretion of angiogenic growth factors and angiogenesis *in vitro*. Tissue Eng **11,** 768, 2005.
21. Leu, A., and Leach, J.K. Proangiogenic potential of a collagen/bioactive glass substrate. Pharm Res **25,** 1222, 2008.
22. Day, R.M., Boccaccini, A.R., Shurey, S., Roether, J.A., Forbes, A., Hench, L.L., and Gabe, S.M. Assessment of polyglycolic acid mesh and bioactive glass for soft-tissue engineering scaffolds. Biomaterials **25,** 5857, 2004.
23. Perea, H., Aigner, J., Heverhagen, J.T., Hopfner, U., and Wintermantel, E. Vascular tissue engineering with magnetic nanoparticles: seeing deeper. J Tissue Eng Regen Med **1,** 318, 2007.
24. Zilberman, Y., Kallai, I., Gafni, Y., Pelled, G., Kossodo, S., Yared, W., and Gazit, D. Fluorescence molecular tomography enables *in vivo* visualization and quantification of nonunion fracture repair induced by genetically engineered mesenchymal stem cells. J Orthop Res, 2007.
25. Humeau, A., Steenbergen, W., Nilsson, H., and Stromberg, T. Laser Doppler perfusion monitoring and imaging: novel approaches. Med Biol Eng Comput **45,** 421, 2007.
26. Phillips, P. Contrast pulse sequences (CPS): imaging nonlinear microbubbles. IEEE 2001 Ultrasonics Symposium **2,** 1739, 2001.
27. Phillips, P., and Gardner, E. Contrast-agent detection and quantification. Eur Radiol **14 Suppl 8,** P4, 2004.
28. Roberts, E.B., Schafer, F., Akhtar, W., Patel, D., Evans, T.R., Coghlan, J.G., Lipkin, D.P., and Davar, J.I. Real-time myocardial contrast dobutamine stress echocardiography in coronary stenosis. Int J Cardiol **113,** 19, 2006.
29. Papadimitropoulos, A., Mastrogiacomo, M., Peyrin, F., Molinari, E., Komlev, V.S., Rustichelli, F., and Cancedda, R. Kinetics of *in vivo* bone deposition by bone marrow stromal cells within a resorbable porous calcium phosphate scaffold: an X-ray computed microtomography study. Biotechnol Bioeng **98,** 271, 2007.
30. Nussenbaum, B., Rutherford, R.B., and Krebsbach, P.H. Bone regeneration in cranial defects previously treated with radiation. Laryngoscope **115,** 1170, 2005.
31. Miao, D., and Scutt, A. Histochemical localization of alkaline phosphatase activity in decalcified bone and cartilage. J Histochem Cytochem **50,** 333, 2002.
32. Lennard, C.M., Patel, A., Wilson, J., Reinhardt, B., Tuman, C., Fenton, C., Blair, E., Francis, G.L., and Tuttle, R.M. Intensity of vascular endothelial growth factor expression is associated with increased risk of recurrence and decreased disease-free survival in papillary thyroid cancer. Surgery **129,** 552, 2001.
33. Keshaw, H., Forbes, A., and Day, R.M. Release of angiogenic growth factors from cells encapsulated in alginate beads with bioactive glass. Biomaterials **26,** 4171, 2005.
34. Richardson, T.P., Peters, M.C., Ennett, A.B., and Mooney, D.J. Polymeric system for dual growth factor delivery. Nat Biotechnol **19,** 1029, 2001.
35. Simmons, C.A., Alsberg, E., Hsiong, S., Kim, W.J., and Mooney, D.J. Dual growth factor delivery and controlled scaffold degradation enhance *in vivo* bone formation by transplanted bone marrow stromal cells. Bone **35,** 562, 2004.
36. Peng, H., Wright, V., Usas, A., Gearhart, B., Shen, H.-C., Cummins, J., and Huard, J. Synergistic enhancement of bone formation and healing by stem cell-expressed VEGF and bone morphogenetic protein-4. J Clin Invest **110,** 751, 2002.
37. Bergeron, E., Marquis, M.E., Chretien, I., and Faucheux, N. Differentiation of preosteoblasts using a delivery system with BMPs and bioactive glass microspheres. J Mater Sci Mater Med **18,** 255, 2007.
38. Deckers, M.M., Karperien, M., van der Bent, C., Yamashita, T., Papapoulos, S.E., and Lowik, C.W. Expression of vascular endothelial growth factors and their receptors during osteoblast differentiation. Endocrinology **141,** 1667, 2000.
39. Midy, V., and Plouet, J. Vasculotropin/vascular endothelial growth factor induces differentiation in cultured osteoblasts. Biochem Biophys Res Commun **199,** 380, 1994.
40. Mayr-Wohlfart, U., Waltenberger, J., Hausser, H., Kessler, S., Gunther, K.P., Dehio, C., Puhl, W., and Brenner, R.E. Vascular endothelial growth factor stimulates chemotactic migration of primary human osteoblasts. Bone **30,** 472, 2002.
41. Villars, F., Bordenave, L., Bareille, R., and Amedee, J. Effect of human endothelial cells on human bone marrow stromal cell phenotype: role of VEGF? J Cell Biochem **79,** 672, 2000.
42. Kaigler, D., Krebsbach, P.H., West, E.R., Horger, K., Huang, Y.C., and Mooney, D.J. Endothelial cell modulation of bone marrow stromal cell osteogenic potential. FASEB J **19,** 665, 2005.
43. Kaigler, D., Krebsbach, P.H., Wang, Z., West, E.R., Horger, K., and Mooney, D.J. Transplanted endothelial cells enhance orthotopic bone regeneration. J Dent Res **85,** 633, 2006.
44. Namiki, A., Brogi, E., Kearney, M., Kim, E.A., Wu, T., Couffinhal, T., Varticovski, L., and Isner, J.M. Hypoxia induces vascular endothelial growth factor in cultured human endothelial cells. J Biol Chem **270,** 31189, 1995.
45. Leong-Poi, H., Christiansen, J., Heppner, P., Lewis, C.W., Klibanov, A.L., Kaul, S., and Lindner, J.R. Assessment of endogenous and therapeutic arteriogenesis by contrast ultrasound molecular imaging of integrin expression. Circulation **111,** 3248, 2005.
46. Heppner, P., and Lindner, J.R. Contrast ultrasound assessment of angiogenesis by perfusion and molecular imaging. Expert Rev Mol Diagn **5,** 447, 2005.
47. Stieger, S.M., Bloch, S.H., Foreman, O., Wisner, E.R., Ferrara, K.W., and Dayton, P.A. Ultrasound assessment of angiogenesis in a Matrigel model in rats. Ultrasound Med Biol **32,** 673, 2006.

Address reprint requests to:
J. Kent Leach, Ph.D.
Department of Biomedical Engineering
University of California, Davis
451 Health Sciences Drive
Davis, CA 95616

E-mail: jkleach@ucdavis.edu

Received: January 11, 2008
Accepted: June 17, 2008
Online Publication Date: September 12, 2008